DE GRUYTER
OPEN

Archives of Hydro-Engineering and Environmental Mechanics
Vol. 64 (2017), No. 1, pp. 17–35
DOI: 10.1515/heem-2017-0002

A Numerical Study of Non-hydrostatic Shallow Flows in Open Channels

Yebegaeshet T. Zerihun

David & James – Engineering and Environmental Consultancy, 204 Albion Road, Victoria 3350, Australia,
E-mail: zyebegaeshet@gmail.com

(Received December 17, 2016; revised June 05, 2017)

Abstract

The flow field of many practical open channel flow problems, e.g. flow over natural bed forms or hydraulic structures, is characterised by curved streamlines that result in a non-hydrostatic pressure distribution. The essential vertical details of such a flow field need to be accounted for, so as to be able to treat the complex transition between hydrostatic and non-hydrostatic flow regimes. Apparently, the shallow-water equations, which assume a mild longitudinal slope and negligible vertical acceleration, are inappropriate to analyse these types of problems. Besides, most of the current Boussinesq-type models do not consider the effects of turbulence. A novel approach, stemming from the vertical integration of the Reynolds-averaged Navier-Stokes equations, is applied herein to develop a non-hydrostatic model which includes terms accounting for the effective stresses arising from the turbulent characteristics of the flow. The feasibility of the proposed model is examined by simulating flow situations that involve non-hydrostatic pressure and/or nonuniform velocity distributions. The computational results for free-surface and bed pressure profiles exhibit good correlations with experimental data, demonstrating that the present model is capable of simulating the salient features of free-surface flows over sharply-curved overflow structures and rigid-bed dunes.

Key words: turbulent flow, numerical modelling, non-hydrostatic pressure, rapidly-varied flow, hydraulic structures

1. Introduction

In practice, rapidly-varied transitions typically involve turbulent flows with substantial vertical curvatures of the streamline that lead to a non-hydrostatic pressure and nonuniform velocity distributions. Many natural open channel flows do possess sharply-curved streamlines as, for instance, at free overfalls; at a channel bed transition from mild to steep slopes; at bed forms; etc. For such flows, higher-order approximations for the vertical profile of the streamline curvature parameters are necessary in order to treat properly the complex transition between hydrostatic and non-hydrostatic flow regimes. Apparently, the shallow-water equations that assume a geometrically mild-slope and negligible vertical acceleration are not always valid

for these types of flow problems (Basco 1987, Blom and Booij 1995, Shimozono and Sato 2016). Furthermore, the validity of the common computational approach based on the gradually-varied flow equation in conjunction with Massé's (1938) singular point method for non-hydrostatic flow situations is questionable (see, e.g., Fenton and Darvishi 2016). Consideration of the effects of nonuniform velocity and non-hydrostatic pressure distributions, and turbulence is very important for overcoming the inherent limitations of the hydrostatic approaches and, hence, accurately predicting the detailed two-dimensional (2D) flow features of a wider class of environmental free-surface flow problems ranging from quasi-hydrostatic to fully non-hydrostatic. From a practical point of view, a higher-order model that incorporates all the geometrical details of a curvilinear streamline is preferred. Such a numerical model enables us to obtain a detailed description of the flow field for a wide range of parameters without resorting to expensive and time consuming physical model tests. It also provides vital information to better understand the rapidly-varying flow regime.

Much effort has been recently devoted to the approximate treatment of the effects of the dynamic pressure due to the curvilinearity of the flow. Hager and Hutter (1984) and Matthew (1991) applied the potential flow theory, with no resistance to the flow, to develop steady Boussinesq-type energy equations. Matthew's (1991) approach was later considered by Castro-Orgaz and Hager (2014) to deal with unsteady free-surface flow problems, which was originally proposed for these problems by Matthew. However, the potential flow approach for the analysis of ideal fluid flow is limited to a short channel length for the energy losses to be neglected and is unable to describe uniform flow. Following Boussinesq's (1877) approach, Fenton and Zerihun (2007), Mohapatra and Chaudhry (2004) and Zerihun (2008) developed the Boussinesq-type momentum equations for modelling rapidly-varied gravity-driven flows with predominant non-hydrostatic pressure distribution effects. Compared to the Boussinesq-type energy equations, these equations are not restricted to irrotationality. Nonetheless, none of the Boussinesq-type energy and momentum equations take into account the effects of turbulence. On the other hand, Serre (1953) extended Boussinesq's approach and developed weakly dispersive but fully nonlinear equations that allow for turbulent friction. The Serre method permits not only flow transition from subcritical to supercritical states, but it also treats the asymptotic conditions at a uniform flow depth. The asymptotic behaviour of a free-surface flow at a normal depth was also considered by Ali and Dey (2016) for modelling open channel flows over a wavy boundary. Recently, Carmo (2013) conducted a numerical case study using an improved Serre-type and Boussinesq-type equations. The results of the study showed that the improved Serre-type equations showed some improvement over the corresponding Boussinesq-type equations in terms of the dispersion characteristics of a wave. Successful numerical applications for Serre-type model using a finite element scheme were also carried out by Tossou (2009). The Dressler (1978) theory, which employs an asymptotic stretching method in an orthogonal bed-fitted curvilinear co-

ordinates, has been applied to analyse open channel flow with curved streamlines. Such an approach was taken by Anh and Hosoda (2007), Berger and Carey (1998a, b) and Dewals et al (2006) to develop higher-order curved-flow equations. Similar to the Boussinesq-type energy equations, however, this approach neither allows vorticity about an axis normal to the plane of flow nor incorporates the effects of turbulence.

Steffler and Jin (1993) introduced an alternative approach based on depth-averaging the Reynolds-averaged Navier-Stokes (RANS) equations with pre-assumed vertical profiles for the pressure and velocity components. They derived the one-dimensional vertically averaged and moment equations by applying both the momentum and moment of momentum principles. Using a similar approach, Jin and Li (1996) developed a depth-averaged moment of momentum model to solve flow problems where the effects of vertical acceleration are significant. However, their model includes undetermined bed pressure parameter which renders the model equations not directly applicable unless information on the bed pressure distribution is incorporated. Using Boussinesq's approximation, Bose and Dey (2007) formulated a higher-order model by depth-averaging the RANS equations. In this approach, the turbulent shear flow was modelled by a power-law velocity profile combined with a standard empirical flow resistance equation. However, the application of Bose and Dey's model is limited to flows with weakly-sloped and curved streamlines. More recently, Zobeyer and Steffler (2012) modelled the 2D vertical plane flows by coupling the one-dimensional depth-averaged equations with the RANS equations. Similar to Steffler and Jin's (1993) approach, this method presents complex system of equations that requires extra computational effort and time.

In spite of the considerable work on the numerical modelling of curvilinear-streamlined flows, relatively little attention has been paid to the development of a higher-order model which incorporates the effects of both the vertical curvatures of the streamline and turbulence. This research work is motivated by the desire to develop a more general form of vertically-averaged model that describes the 2D structure of a curvilinear flow field accurately. The proposed method is based on the vertical integration of the RANS equations with the inclusion of the power-law model for the vertical profile of the horizontal velocity component, and yields a flow model that incorporates vertically-averaged turbulent stresses and a higher-order dynamic pressure correction. In contrast to Jin and Li's (1996) equations, the model does not include any undetermined parameter related to the bed pressure. This study is also undertaken to investigate the applicability of the proposed model to practical free-surface flow problems where the ratio of the vertical to horizontal scales of motion is not sufficiently small. These problems include free-surface flows over symmetrical and asymmetrical humps, and nonuniform flows over dredged trenches and dunes. The numerical solutions of such quasi-hydrostatic and non-hydrostatic flow problems can provide useful information for examining the effects of the dynamic pressure of the flow on the performance of the model. It is important to emphasise that the method

presented here allows a systematic numerical investigation of the rapidly-varied flow transitions in open channels where the vertical acceleration plays a significant role.

The paper is organised as follows. In the following sections, the derivation of the governing equations is presented first, followed by a brief discussion of the spatial discretisation of the equations and extension of the numerical model. The solution procedures for the resulting nonlinear discretised equations with reference to the case studies and the associated boundary conditions are also depicted. A brief discussion of the model results is presented by comparing them with experimental data. The paper is ended with conclusive remarks.

2. Numerical Methodology

2.1. Governing Equations

A curvilinear-streamlined, incompressible, free-surface flow is considered for analyses. A Cartesian coordinate system such that x is horizontal along the channel, y is horizontal in the transverse direction and z is vertically upward is chosen, as shown schematically in Figure 1. For 2D flow, the continuity and the RANS equations can be written as (see, e.g., French 2007, White 2011)

$$\frac{\partial \overline{u}}{\partial x} + \frac{\partial \overline{w}}{\partial z} = 0, \tag{1}$$

$$\frac{\partial \overline{u}}{\partial t} + \overline{u}\frac{\partial \overline{u}}{\partial x} + \overline{w}\frac{\partial \overline{u}}{\partial z} + \frac{1}{\rho}\frac{\partial \overline{p}}{\partial x} - \frac{1}{\rho}\left(\frac{\partial \tau_{xz}}{\partial z} + \frac{\partial \sigma_x}{\partial x}\right) = 0, \tag{2}$$

$$\frac{\partial \overline{w}}{\partial t} + \overline{u}\frac{\partial \overline{w}}{\partial x} + \overline{w}\frac{\partial \overline{w}}{\partial z} - G_z + \frac{1}{\rho}\frac{\partial \overline{p}}{\partial z} - \frac{1}{\rho}\left(\frac{\partial \tau_{zx}}{\partial x} + \frac{\partial \sigma_z}{\partial z}\right) = 0, \tag{3}$$

where $\overline{u}$ and $\overline{w}$ denote the time-mean horizontal and vertical velocity components, respectively; G_z is the body force per unit mass; ρ is the density of the fluid; $\overline{p}$ is the time-mean pressure; σ and τ refer to the total normal and shear stresses, respectively and t is the time.

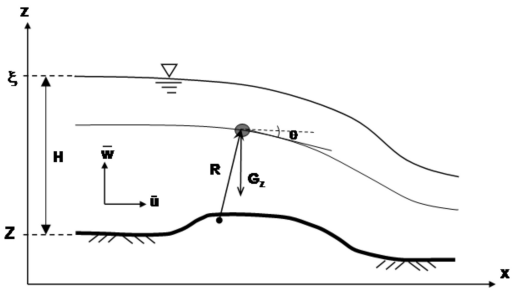

Fig. 1. Definition sketch of turbulent free-surface flow over a curved bed

The distribution of the time-mean horizontal velocity across the flow depth is approximated by the power-law velocity profile for a turbulent flow as

$$\overline{u} = \frac{\omega_0 q}{H}\left(\eta^{1/N}\right), \tag{4}$$

$$\eta = \frac{z - Z}{\xi - Z}, \tag{5}$$

where q is the unit discharge; ξ is the free-surface elevation; η is a dimensionless vertical coordinate; z is the vertical elevation of a point in the flow field; Z is the channel bed elevation; H is the local flow depth measured vertically; N is the reciprocal of exponent and $\omega_0 = (N + 1)/N$. The value of the reciprocal of exponent varies from 4 to 12 depending upon the boundary friction and cross-sectional shape (see, e.g., Chen 1991), and it can be determined from the measured time-mean velocity data. By applying Leibnitz's rule, the vertical integration of Equation (1) becomes

$$\int_z^\xi \frac{\partial \overline{u}}{\partial x} dz + \int_z^\xi \frac{\partial \overline{w}}{\partial z} dz = \frac{\partial}{\partial x}\int_z^\xi \overline{u}(z)\, dz + \overline{u}(z)\, z_x - \overline{u}(\xi)\frac{\partial \xi}{\partial x} + \overline{w}_s - \overline{w} = 0. \tag{6}$$

Inserting Equation (4) into Equation (6) and applying the free-surface kinematic boundary condition, $\overline{w}_s = \partial H/\partial t + (\partial \xi/\partial x)\,\overline{u}_s$ results for the vertical velocity distribution in

$$\overline{w} = \frac{\partial H}{\partial t}\left(\eta^{(N+1)/N}\right) + \frac{\omega_0 q}{H}\frac{\partial H}{\partial x}\left(\eta^{(N+1)/N}\right) + \frac{\omega_0 q Z_x}{H}\left(\eta^{1/N}\right), \tag{7}$$

where $\overline{u}_s\ (= \omega_0 q/H)$ and $\overline{w}_s$ are the horizontal and vertical components of the velocity at the free-surface, respectively.

In order to describe the local flow characteristics in terms of depth and discharge, the continuity equation and the RANS equation for the streamwise x-direction motion are vertically integrated from the bed to the free-surface by applying Leibnitz's rule and making use of Equations (4) and (7). The following kinematic and dynamic boundary conditions are used to eliminate parameters evaluated at the free-surface and bed:

$$\overline{w}(Z) = \overline{u}(Z)\, Z_x, \tag{8a}$$

$$\sigma(\xi) = \tau(\xi) = 0, \tag{8b}$$

$$\tau(Z) = \tau_b. \tag{8c}$$

The resulting vertically-averaged equations then become

$$\frac{\partial H}{\partial t} + \frac{\partial q}{\partial x} = 0, \tag{9a}$$

$$\frac{\partial q}{\partial t} + \frac{\omega_0 q}{H}\left(\frac{\omega_1 + 1}{\omega_1}\right)\frac{\partial q}{\partial x} - \frac{\omega_0^2 q^2}{H^2 \omega_1}\frac{\partial H}{\partial x} + \frac{1}{\rho}\int_Z^{\xi}\frac{\partial \overline{p}}{\partial x}dz + \frac{1}{\rho}\left(\tau_b - \frac{\partial H\overline{\sigma}_x}{\partial x}\right) = 0, \quad (9b)$$

where $\omega_1 = (N+2)/N$; τ_b is the bed shear stress and $\overline{\sigma}_x$ is the vertically-averaged normal stress.

In most practical open-channel flow problems, the rates of change of quantities with time are much slower than the apparent acceleration of a fluid particle following a curvilinear path (Fenton and Zerihun 2007). Furthermore, for fully developed turbulent flows, the variation of the shear stress in the streamwise x-direction may be considered to be small when compared to that in the vertical direction. Using the former approximation in Equation (3), the vertical acceleration of the flow becomes

$$\overline{u}\frac{\partial \overline{w}}{\partial x} + \overline{w}\frac{\partial \overline{w}}{\partial z} = \kappa\frac{\overline{u}^2}{\cos^3\theta} = \overline{u}^2\,\lambda, \quad (10)$$

where κ $(= 1/R)$ is the curvature of the streamline; R is the radius of curvature and θ is the angle of inclination of the streamline with the horizontal axis. To proceed, the vertical distribution of the streamline geometry parameter, λ, must be specified. For simplicity, a linear profile

$$\lambda = \lambda_b + (\lambda_s - \lambda_b)\,\eta, \quad (11)$$

is assumed. The subscripts b and s refer to magnitudes of a parameter at the channel bed and free-surface, respectively. Inserting Equations (4) and (10) into Equation (3) and then vertically integrating the resulting expression from z to ξ leads to the time-mean pressure distribution equation for flow in a rectangular channel

$$\frac{\overline{p}}{\rho g} = H(1-\eta) + \frac{\omega_0^2 q^2 Z_{xx}}{gH\omega_1}\left(1 - (\eta)^{(N+2)/N}\right) + \frac{\omega_0^2 q^2}{gH(\omega_1+1)}\frac{d^2H}{dx^2}\left(1 - (\eta)^{(2N+2)/N}\right) + \frac{\sigma_z}{\rho g}. \quad (12)$$

The first term on the right-hand side (RHS) of Equation (12) is the hydrostatic pressure and the other three terms account for the effects of the vertical curvatures of the streamline and turbulence. The contribution of the last term on the RHS of this equation is significant only for open channel flows with strong turbulent eddies. For the case of gradually-varying free-surface flow with negligible vertical acceleration and weak turbulent characteristics, the free-surface and bed curvatures terms vanish ($d^2\xi/dx^2 = Z_{xx} = 0$). Under this flow condition, Equation (12) reduces to the well-known hydrostatic pressure equation.

For 2D flow in the vertical plane, the free-surface is nearly horizontal in the cross-channel direction so that the pressure is not a function of y. By applying Leibnitz's rule, the integral of the pressure gradient term in Equation (9b) may be written as

$$\frac{1}{\rho}\int_{Z}^{\xi}\frac{\partial \overline{p}}{\partial x}dz = \frac{1}{\rho}\left(\frac{\partial}{\partial x}\int_{Z}^{\xi}\overline{p}\,(z)\;dz + \overline{p}\,(Z)\,Z_x - \overline{p}\,(\xi)\,\frac{\partial \xi}{\partial x}\right). \tag{13}$$

Using Equation (12) in Equation (13) and then substituting the resulting expression in Equation (9b) yields the following equation for flow in a rectangular channel after employing the dynamic boundary condition, $\overline{p}\,(\xi) = 0$, at the free-surface:

$$\begin{aligned}&\frac{\partial q}{\partial t} + \frac{\omega_0 q}{H}\left(\frac{\omega_1+1}{\omega_1}\right)\frac{\partial q}{\partial x} + \omega_0^2 q\left(\frac{2Z_{xx}}{(\omega_1+1)} + \frac{2}{(\omega_1+2)}\frac{\partial^2 H}{\partial x^2}\right)\frac{\partial q}{\partial x}\\ &+\left(gH - \frac{\omega_0^2 q^2}{H^2\omega_1}\right)\frac{\partial H}{\partial x} + \frac{\omega_0^2 q^2 Z_x}{H\,(\omega_1+1)}\frac{\partial^2 H}{\partial x^2} + \frac{\omega_0^2 q^2}{(\omega_1+2)}\frac{\partial^3 H}{\partial x^3} + \frac{\omega_0^2 q^2 Z_{xx} Z_x}{H\omega_1}\\ &+\frac{\omega_0^2 q^2 Z_{xxx}}{(\omega_1+1)} + \frac{1}{\rho}\left(\frac{\partial H\overline{\sigma}_z}{\partial x} - \frac{\partial H\overline{\sigma}_x}{\partial x}\right) + gHZ_x + \frac{\tau_b}{\rho} = 0,\end{aligned} \tag{14}$$

where Z_x, Z_{xx} and Z_{xxx} are the first, second and third derivatives of the bed profile, respectively. Neglecting the effect of turbulence and assuming a constant vertical profile for the horizontal velocity component ($\omega_0 = \omega_1 = 1$), Equation (14) degenerates to a flow equation structurally similar to those given by Fenton and Zerihun (2007) and Zerihun (2008).

For steady flow, the discharge is constant, so that $\partial H/\partial t = \partial q/\partial x = \partial q/\partial t = 0$. Using these relationships in Equation (14), the following equation is obtained:

$$\begin{aligned}&\frac{\omega_0^2 q^2}{(\omega_1+2)}\frac{d^3 H}{dx^3} + \frac{\omega_0^2 q^2 Z_x}{H\,(\omega_1+1)}\frac{d^2 H}{dx^2} + \left(gH - \frac{\omega_0^2 q^2}{H^2\omega_1}\right)\frac{dH}{dx} + \frac{\omega_0^2 q^2 Z_{xx} Z_x}{H\omega_1}\\ &+\frac{\omega_0^2 q^2 Z_{xxx}}{(\omega_1+1)} + \frac{1}{\rho}\left(\frac{dH\overline{\sigma}_z}{dx} - \frac{dH\overline{\sigma}_x}{dx}\right) + gHZ_x + \frac{\tau_b}{\rho} = 0.\end{aligned} \tag{15}$$

Equation (15) incorporates terms that account for the effects of both the vertical curvatures of the streamline and turbulence, and their associated consequences on the velocity and pressure distributions. The bed shear stress can be modelled by using the Darcy-Weisbach equation as (Fenton and Zerihun 2007)

$$\frac{\tau_b}{\rho} = \frac{f q^2}{8H^2}\left(1 + Z_x^2\right), \tag{16}$$

where f is the Darcy-Weisbach friction factor which can be computed using the formula given by Haaland (1983). The preceding method demonstrates that a weakly-curved flow assumption is not really required to develop such types of governing equations. In this study, Equations (4), (7), (12) and (15) will be applied to simulate the salient characteristics of curvilinear turbulent flows in rectangular channels. The solutions of the additional turbulent stress terms in Equation (15) require a turbulence closure model, which will be discussed in the following section. It is worth noting that modelling the free-surface as a freely deformable air-water interface of a two-phase flow is beyond the scope of the present work.

2.1.1. Turbulence Modelling

The eddy-viscosity turbulence model has been incorporated in the current numerical model. This turbulence model is easy to implement and, with careful application, can provide practically good results for turbulent open channel flows (Ferziger and Peric 2002). The vertically-averaged normal stresses appearing in Equations (14) and (15) are approximated according to the Boussinesq eddy-viscosity hypothesis as follows (Boussinesq 1877, van Rijn 2011):

$$\overline{\sigma}_x = \frac{1}{H}\int_Z^{\xi} \sigma_x dz = 2\rho\,(\nu_m + \overline{\nu}_x)\left(\frac{1}{H}\frac{dq}{dx} - \frac{\omega_0 q}{H^2}\frac{d\xi}{dx}\right), \tag{17}$$

$$\overline{\sigma}_z = \frac{1}{H}\int_Z^{\xi} \sigma_z dz = 2\rho\,(\nu_m + \overline{\nu}_z)\left(\frac{\overline{w}_s - \overline{w}_b}{H}\right), \tag{18}$$

where $\overline{\nu}_x$ and $\overline{\nu}_z$ are the vertically-averaged kinematic eddy viscosities or turbulent exchange coefficients in the horizontal and vertical directions, respectively; ν_m is the molecular kinematic viscosity and $\overline{w}_b$ is the time-mean vertical velocity at the bed. The kinematic eddy viscosities are the only turbulent parameters directly affecting the solutions of the governing equations and need to be predicted accurately by the turbulence model. In this work, the turbulent exchange coefficients are calculated by using the parabolic eddy-viscosity model (Elder 1959, Fischer et al 1979, Rodi 1993)

$$\overline{\nu}_x = \alpha_t C_s \mathrm{K} U_* H, \tag{19a}$$

$$\overline{\nu}_z = C_s \mathrm{K} U_* H, \tag{19b}$$

$$U_* = \sqrt{\frac{\tau_b}{\rho}}, \tag{19c}$$

where $C_s = 1/6$; K is von Kármán's constant (0.41); U_* is the boundary shear velocity and α_t is an empirical coefficient which varies between 1 and 10. Equations (17)–(19) are numerically coupled with Equations (12) and (15) for the complete solutions of the turbulent free-surface flow problems with curvilinear streamlines.

2.1.2. Boundary Conditions

The numerical solutions of the turbulent flow problems using the model equation require three external boundary conditions to be specified at the two extreme sections of the solution domain. At the upstream boundary, a constant flow depth is specified and then the slope of the free-surface, S_H, is computed from the gradually-varied flow equation,

$$S_H = \frac{dH}{dx} = \frac{S_0 - S_f}{1 - \beta F^2}, \tag{20}$$

where F is the Froude number; β refers to the Boussinesq coefficient; S_f denotes the friction slope and S_0 is the bed slope. At the downstream boundary, the flow depth is specified and remained unchanged during the computations.

2.2. Numerical Method and Simulation Procedure

A numerical method is applied since closed-form solutions are not available for the above nonlinear differential equations. Zerihun's (2004) numerical model, which was developed for simulating transcritical free-surface flows, is extended here to solve the rapidly-varied turbulent flow problems. Equation (15) may be rewritten in a form suitable for discretisation as

$$\left(\frac{d^3H}{dx^3}\right)_j + \varsigma_{0,j}\left(\frac{d^2H}{dx^2}\right)_j + \varsigma_{1,j}\left(\frac{dH}{dx}\right)_j + \varsigma_{2,j} + \varsigma_{3,j} = 0, \tag{21}$$

where $\varsigma_{0,j}$, $\varsigma_{1,j}$, $\varsigma_{2,j}$ and $\varsigma_{3,j}$ are the associated nonlinear coefficients at node j and are given by:

$$\varsigma_{0,j} = \frac{Z_{x,j}\,(\omega_1 + 2)}{H_j\,(\omega_1 + 1)}, \tag{22a}$$

$$\varsigma_{1,j} = \frac{gH_j\,(\omega_1 + 2)}{q_j^2\omega_0^2} - \frac{(\omega_1 + 2)}{H_j^2\omega_1}, \tag{22b}$$

$$\varsigma_{2,j} = \frac{Z_{xxx,j}\,(\omega_1 + 2)}{(\omega_1 + 1)} + \frac{Z_{x,j}Z_{xx,j}\,(\omega_1 + 2)}{H_j\omega_1} + \frac{gH_jZ_{x,j}\,(\omega_1 + 2)}{q_j^2\omega_0^2}, \tag{22c}$$

$$\varsigma_{3,j} = \frac{(\omega_1 + 2)}{\rho q_j^2\omega_0^2}\left[\tau_b + (\overline{\sigma}_z - \overline{\sigma}_x)\frac{dH}{dx} + \left(\frac{d\overline{\sigma}_z}{dx} - \frac{d\overline{\sigma}_x}{dx}\right)H\right]_j. \tag{22d}$$

An efficient numerical scheme, whose solutions are not significantly affected by the truncation errors, can be developed by discretising Equation (21) with higher-order accurate finite difference formulae (see, e.g., Ferziger and Peric 2002). Hence, a consistent discretisation of the spatial derivative terms of this equation using the

four-point finite difference approximations (Abramowitz and Stegun 1972) gives the following equation:

$$\begin{aligned} &6\varsigma_{3,j}(\Delta x)^3 + 6\varsigma_{2,j}(\Delta x)^3 + H_{j-2}\left(-6 + \varsigma_{1,j}(\Delta x)^2\right) \\ &+H_{j-1}\left(18 + 6\varsigma_{0,j}\Delta x - 6\varsigma_{1,j}(\Delta x)^2\right) + H_j\left(-18 - 12\varsigma_{0,j}\Delta x + 3\varsigma_{1,j}(\Delta x)^2\right) \\ &+H_{j+1}\left(6 + 6\varsigma_{0,j}\Delta x + 2\varsigma_{1,j}(\Delta x)^2\right) = 0, \end{aligned} \tag{23}$$

where Δx is the step size. Since the flow depth at the inflow section ($j = 0$) is known, the depth at the imaginary node ($j = -1$) can be determined from the known free-surface slope, S_H, at $j = 0$. Using the discretised and expanded forms of Equations (20) and (23) at the inflow section, the following implicit finite difference equation is obtained for predicting the depth at $j = -1$:

$$\begin{aligned} &H_{-1}(-18 + 6\varsigma_{0,0}\Delta x) - H_0(12\varsigma_{0,0}\Delta x) + H_1(18 + 6\varsigma_{0,0}\Delta x) \\ &+6S_H\left(-6\Delta x + \varsigma_{1,0}(\Delta x)^3\right) + 6\varsigma_{2,0}(\Delta x)^3 + 6\varsigma_{3,0}(\Delta x)^3 = 0. \end{aligned} \tag{24}$$

The above nonlinear algebraic equations are solved numerically by treating the flow problem using both the upstream and downstream boundary conditions. An iterative method is utilised for solving the problem, which starts from an initial prediction for the free-surface position using the Bernoulli and continuity equations. Then, to simulate the free-surface profile, Equations (17)–(19) and (23) are applied at different nodal points within the solution domain and results in a system of nonlinear algebraic equations. These equations, together with Equation (24) and the known boundary values at the inflow and outflow sections, are solved simultaneously by the Newton-Raphson method with a numerical Jacobian matrix. A test for convergence is made using the following criterion:

$$\frac{\sum_{j=1}^{m}\left|\delta H_j\right|}{\sum_{j=1}^{m}\left|H_j\right|} \leq \Gamma_0, \tag{25}$$

where δH_j is the correction depth in any stage of the iteration process at nodal point j; m is the total number of nodes in the solution domain excluding boundary nodes at the inflow and outflow sections and $\Gamma_0 = 10^{-6}$ is the specified convergence tolerance.

For discretising the derivative term in the pressure equation, a similar finite difference approximation is inserted into Equation (12) after setting η equal to zero for the pressure on the bed. The discretised equation is then applied to compute the bed pressure profiles at different nodal points using the known flow depths. Applications of the preceding system of equations, including step size independence assessment, for non-hydrostatic open channel flow problems are given in the succeeding section.

3. Comparison and Analysis of Results

3.1. Velocity Distribution Parameter

As stated, the determination of the reciprocal of exponent in the power-law velocity profile is an essential requirement to model the selected test problems. Lyn's (1993) experimental results for free-surface flow over triangular profile dunes are selected for this purpose. A train of sand-plastered wooden dunes, of wavelength $L = 150$ mm and height $H_D = 12$ mm, was used to conduct the experiments (for details, see Figure 2a). The slopes of the stoss-side and lee-side of this profile were 5° and 45°, respectively. Measurements of mean and turbulence characteristics were obtained using two-component Laser Doppler Velocimetry. Figure 2b shows the variation of the normalised horizontal velocity, Ω ($\Omega = \overline{u}/U$; $U = q/H$ is the depth-averaged streamwise horizontal velocity), with the normalised vertical distance above the bed, η, at four measurement stations. As shown in this figure, a value of $N = 7$ for the power-law profile provides a fairly good agreement with experimental data, with a mean relative error of 8.4%. The computed standard deviation and coefficient of determination for the fitted profile curve are 0.08 and 0.88, respectively. The overall analysis results indicate that the predicted velocity profile slightly deviates from the measured data near the bed of the dune ($\eta < 0.20$). This is a consequence of flow reversal near the bed which modifies the velocity distribution in the deceleration zone. For turbulent flows over rough bed-forms with small amplitude to wavelength ratios, the effect of flow separation or recirculation is insignificant. Also, the result of a numerical study conducted by Ghamry and Steffler (2002) suggests that applying different types of approximations for the shape of the velocity distribution does not affect the overall accuracy of the model results significantly, especially for global flow characteristics. All these facts substantiate that the proposed one-seventh power-law adequately describes the velocity distribution, allowing the non-hydrostatic model to simulate satisfactorily the 2D features of the rapidly-varied turbulent flows.

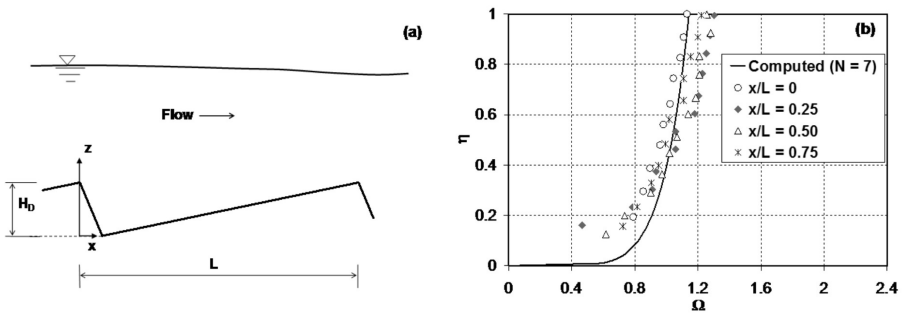

Fig. 2. (a) schematic of a dune bed form; (b) longitudinal velocity distributions

3.2. Effect of Step Size Refinement

Measurements for free-surface and bed pressure profiles for model validations are obtained from the experiments performed by Sivakumaran (1981). The experiments were conducted in a rectangular, horizontal flume, 9.15 m long, 650 mm high and 300 mm wide. The flume was made of a steel frame with glass windows on both vertical sides and its bed was constructed using a 15 mm thick plywood. A symmetrical and asymmetrical humps made of polyvinyl chloride (PVC) were tested. A point gauge of reading accuracy 0.10 mm was used to measure the flow depth along the centreline of the flume. Similarly, the bed pressure was observed at different tapping points along the centreline of the curved beds using vertical piezometers of accuracy 1 mm. Full details of the description of the experimental system can be found in Sivakumaran (1981). For this test problem, a smooth boundary resistance method was applied to compute the friction factors.

In order to assess the effect of spatial step size refinement on the accuracy of the model results, free-surface flows with curvilinear streamlines were simulated using various step sizes. Due to similarity of results, only the simulation results for flow over a symmetrical hump are presented here. Figure 3 shows the free-surface and bed pressure profiles simulated by the proposed model for step sizes 20 mm, 40 mm, 60 mm, 80 mm and 100 mm. The overall simulation result for free-surface profile was not significantly affected until the step size exceeded the depth at the outflow section. When the spatial step size exceeded this threshold value, the model results showed appreciable deviation from measurements in the subcritical flow region. As shown in the figure, the finest discretisation ($\Delta x \leq 40$ mm) yielded better numerical results without any surface undulation upstream of the axis of symmetry of the hump. At the coarsest discretisation, the result for the bed pressure profile (p_b is the bed pressure) was significantly affected in the region upstream of the critical section. Hence, only model results obtained for a finer step size are presented hereinafter.

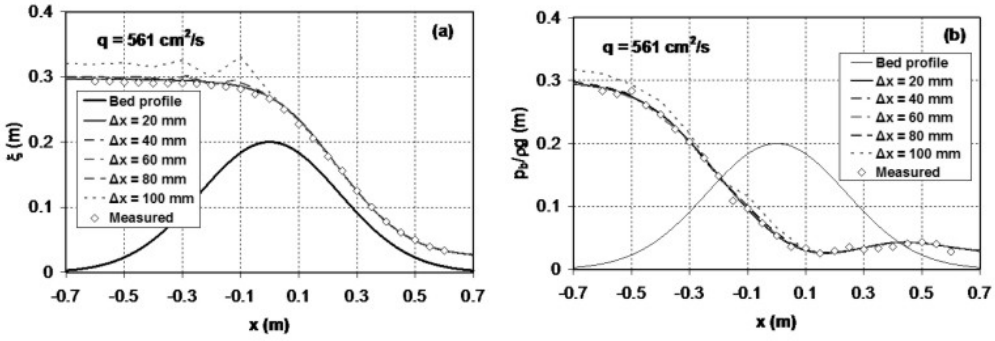

Fig. 3. Numerical simulation results for various spatial step sizes: (a) free-surface profile; (b) bed pressure profile

3.3. Predictions of a Non-hydrostatic Free-surface Flow

3.3.1. Sivakumaran's (1981) experiment

The performance of the model is further assessed by simulating strongly-curved flows over symmetrical and asymmetrical humps and the results are compared with Sivakumaran's (1981) experimental data in Figures 4 and 5. For both cases, the model results for the upstream free-surface profile show close agreement with experimental data, revealing that the discharge capacity of such an overflow structure can be estimated accurately by this model (see Figures 4a and 5a). At the crest of the humps ($dZ/dx \cong 0$), the model accurately predicts the location and magnitude of the critical flow depth. Immediately downstream of the critical section where the curvature of the free-surface is substantial, the free-surface slope and elevations are correctly simulated. Similar performance results can be seen in the quasi-uniform supercritical flow region as well as in the vicinity of the toe of the humps. The computational results demonstrate that the proposed model accurately reproduces the non-hydrostatic flow features regardless of the degree of the vertical curvatures of the streamline.

As illustrated in Figures 4b and 5b, the computed bed pressure compares well with measured data in the flow region upstream of the critical section. A minor difference between the measured and predicted results can be seen from these figures farther downstream of the crest of the humps. As described by Sivakumaran (1981), the observed bed pressure in this flow region might have some systematic errors due to small local turbulence and curvature error introduced by the flat end piezometer tappings. It is clear from Figures 4 and 5 that the pressure distribution is definitely non-hydrostatic in the flow regions around the crest and toe of the humps due to the substantial vertical curvatures of the free-surface and bed.

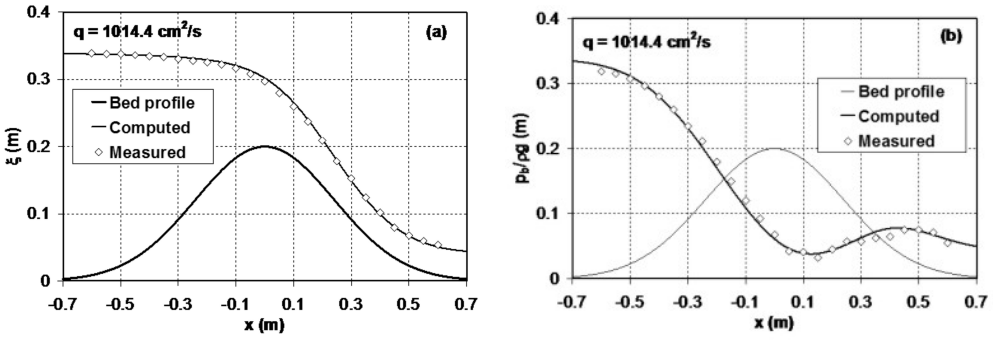

Fig. 4. Curvilinear transcritical flow over a symmetrical hump: (a) free-surface profile; (b) bed pressure profile

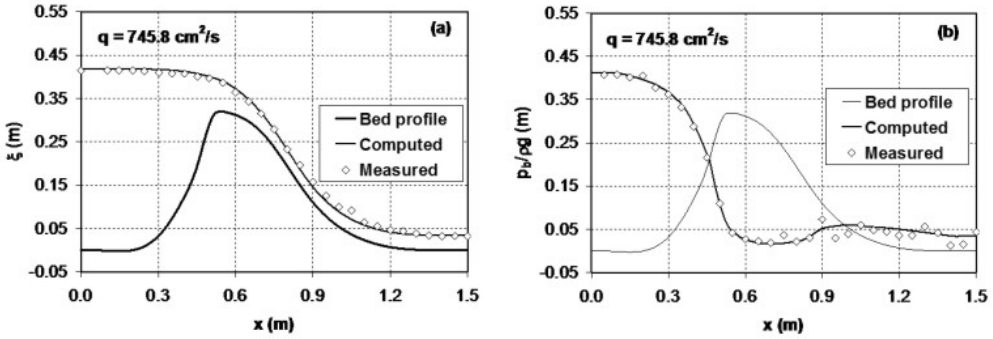

Fig. 5. Curvilinear transcritical flow over an asymmetrical hump: (a) free-surface profile; (b) bed pressure profile

3.3.2. The Experiment of Delft Hydraulics Laboratory (1980)

The experimental data of Delft Hydraulics Laboratory (1980) for turbulent flows over dredged trenches were employed here. The experiments were performed in trenches which were installed in a rectangular flume, 17 m long, 500 mm wide and 700 mm deep. The bottom slopes of the trench were varied from 7.1° to 26.6° and the equivalent roughness heights of the bed were between 4 mm and 25 mm. A Laser Doppler Velocimetry and a point gauge were used to measure the velocity and free-surface profiles, respectively. The data of runs T4 and T14 were used to validate the model results.

For this test problem, the free-surface profiles were simulated by specifying experimentally determined free-surface slopes at the inflow section of the computational domain. Also, the friction factors for the trench bed were estimated using the suggested equivalent roughness heights of 6.5 mm and 4.5 mm for the T4 and T14 runs, respectively. Figure 6 depicts the comparison of the model results for free-surface profile in the streamwise direction with experimental data. For the considered quasi-hydrostatic flow condition, the numerical results correspond well to the experimental data of Delft Hydraulics Laboratory (1980). As expected, the effect of the vertical acceleration plays an important role only in the flow region near the upstream and downstream inclined faces of the trench.

3.3.3. Cottino's (1993) Experiment

The experimental results of Cottino (1993) are invoked to test the capability of the proposed model to simulate flows over rigid-bed dunes. The experiments were conducted in a 380 mm wide flume with a 9 m long test section, set at a longitudinal slope of 0.2%, at the Lower Laboratory of the University of the Witwatersrand. A series of six identical, sand-plastered triangular dunes, of constant lee-side slope 30° and height H_D = 45 mm, was fixed to the floor of the flume. The dunes were constructed

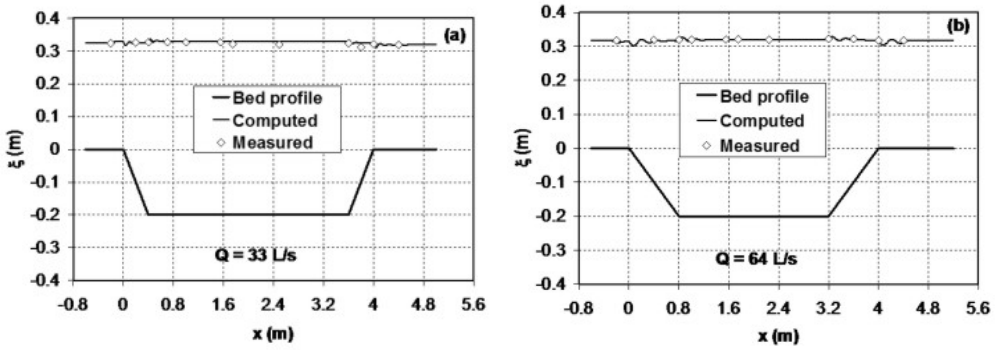

Fig. 6. Free-surface profiles for flow over dredged trenches for two different values of discharge, Q and maximum bottom slope: (a) slope = 26.6°; (b) slope = 14°

of galvanised steel sheeting attached to wooden supports and were roughened by plastering nearly uniform size of different grades of sand over the surface. Four different triangular-shaped dunes with different surface roughnesses were tested for a range of flow conditions. The slope of the stoss-side of these dunes was varied by using different wavelengths, as indicated in Table 1. The bed pressure and free-surface profiles measurements were taken along the centreline of the third dune in a train of six dunes using a piezometer tube connected to a vertical manometer and a point gauge, respectively. Full details of the description of the experimental system can be found in Cottino (1993) and James and Cottino (1995). The experimental results for bed-geometry shapes G2 and G4 (for details, see Table 1) were selected to validate the model results.

Table 1. Details of the rigid-bed dune geometry and surface roughness

Geometry	L (mm)	D_{50}(mm)	Stoss-side angle
G2	900	3.05	3.13°
G4	1500	1.6	1.80°

For this test problem, the computational domain was carefully chosen in order to set the inflow and outflow sections at a fully developed quasi-uniform flow region. This was achieved by extending the computational length upstream of the first and downstream of the sixth dunes to 1.5 m. The friction factors for the bed shear stress were estimated by taking the median size diameter (D_{50}) as an equivalent roughness height for the uniform sand-grain bed (see, e.g., Meyer-Peter and Müller 1948). The normalised free-surface profiles for different flow conditions for dune types G2 and G4 are illustrated in Figures 7a and 8a. The computational results show a satisfactory agreement with experimental data. In all cases, the free-surface profiles are invariably out of phase with the bed-form profile, which is a typical characteristic of subcritical flow over dunes. As can be seen from these figures, free-surface undulations persist

at higher discharges due to the effects of the geometric shape of the bed forms and turbulent eddies in the deceleration zone ($x/L \leq 0.2$).

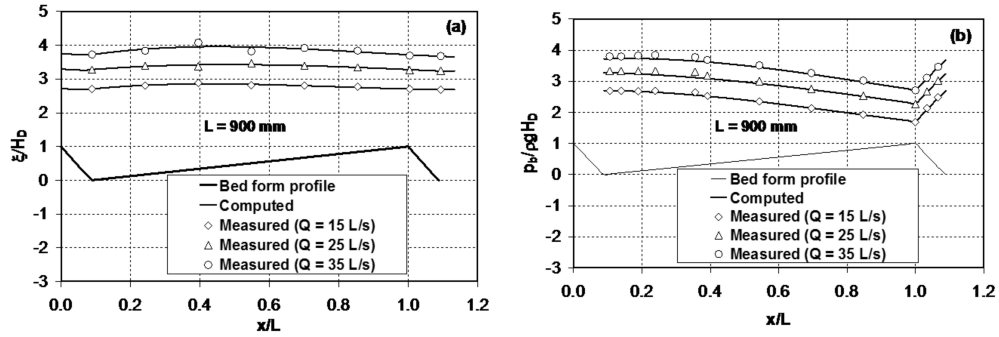

Fig. 7. Flow over a rigid-bed dune with a dune height to wavelength ratio of 0.05: (a) free-surface profile; (b) bed pressure profile

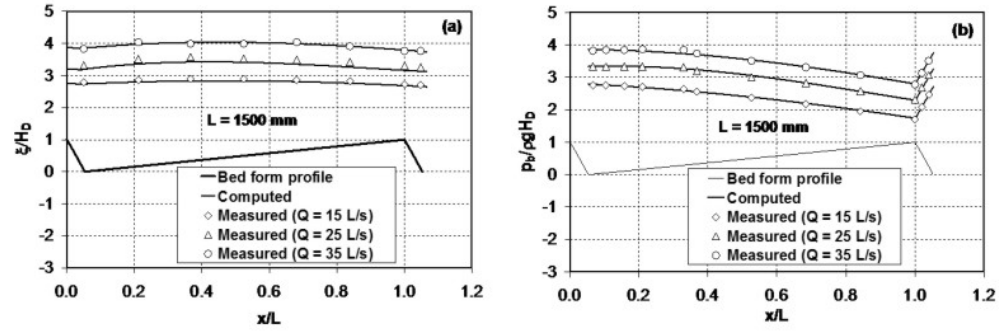

Fig. 8. Flow over a rigid-bed dune with a dune height to wavelength ratio of 0.03: (a) free-surface profile; (b) bed pressure profile

The variation of the normalised bed pressure with the non-dimensional horizontal distance is shown in Figure 7b and 8b. As in the test case of curvilinear flow over curved beds, the computational results are in good agreement with experimental data. It is evident from these figures that the bed pressure is nearly constant within the deceleration zone ($0.06 \leq x/L < 0.2$) and attains its minimum value at the crest of the dune ($x/L = 1$). This flow feature is accurately mimicked by the proposed model. For this numerical experiment, the effect of the streamline vertical curvature might not be significant in the region of accelerated flow. The overall simulation results indicate that the global flow characteristics of free-surface flows over dunes cannot be accurately modelled by using a traditional approach which treats the dunes as a roughness element without accounting for the effects of form resistance. Such a classical modelling approach provides a quasi-uniform flow solution to the problem due to the loss of information on the vertical structure of the bed-form geometry.

4. Concluding Remarks

A novel approach, stemming from the vertical integration of the Reynolds-averaged Navier-Stokes equations with the assumption of a power-law of velocity distribution, was applied to develop a non-hydrostatic model for 2D turbulent free-surface flows. The proposed model includes vertically-averaged turbulent stresses which make it completely different from the Boussinesq-type models and utilises the first-order accurate turbulence closure model. The governing differential equations were discretised by means of a finite difference scheme. Solutions to the resulting nonlinear algebraic equations were obtained using the Newton-Raphson iterative solver with a numerical Jacobian matrix. The feasibility of the model was examined by simulating flow situations that involve non-hydrostatic pressure and/or nonuniform velocity distributions.

For the case of curvilinear flows over symmetrical and asymmetrical humps, the model reproduced flow transition from subcritical to supercritical states accurately regardless of the degree of the vertical curvatures of the streamline. The results of the simulation suggested that the discharge capacity of these types of overflow structures can be estimated reasonably well by the proposed model. For the quasi-hydrostatic flows over rigid-bed dunes, the free-surface profile results showed good correlations with experimental data and were invariably out of phase with the bed-form profile, which is a typical characteristic of subcritical flow over dunes. Furthermore, the bed pressure profile, which was at a constant maximum within the deceleration zone and at a minimum at the dune crest, was correctly simulated by the model. The overall comparison results demonstrate that such salient global flow characteristics cannot be modelled by using a traditional approach which treats the dunes as a roughness element rather than a part of large bed-geometry features. In general, the proposed non-hydrostatic model was found to be accurate, and gave reasonably good results for all cases studied. It is concluded that this model can be applied to solve other rapidly-varied turbulent flow problems in which a clear picture of the 2D characteristics of the flow field is sought.

References

Abramowitz M. and Stegun I. A. (1972) *Handbook of Mathematical Functions with Formulas, Graphs and Mathematical Tables*, 10th ed., Wiley, New York, NY.

Ali S. and Dey S. (2016) Theory of turbulent flow over a wavy boundary, *J. Hydr. Eng.*, **142** (6), 10.1061/(ASCE)HY.1943-7900.0001125.

Anh T. N. and Hosoda T. (2007) Depth-averaged model of open-channel flows over an arbitrary 3D surface and its applications to analysis of water surface profile, *J. Hydr. Eng.*, **133** (4), 350–360.

Basco D. R. (1987) *Computation of Rapidly-varied, Unsteady, Free-surface Flow, Water Resources Investigation Report No. 83–4284*, U.S. Geological Survey, Reston, VA.

Berger R. C. and Carey G. F. (1998a), Free-surface flow over curved surfaces-Part I: Perturbation analysis, *Int. J. Numer. Methods Fluids*, **28** (2), 191–200.

Berger R. C. and Carey G. F. (1998b), Free-surface flow over curved surfaces-Part II: Computational model, *Int. J. Numer. Methods Fluids*, **28** (2), 201–213.

Blom P. and Booij R. (1995) Turbulent free-surface flow over sills, *J. Hydr. Res.*, **33** (5), 663–682.

Bose S. and Dey S. (2007) Curvilinear flow profiles based on Reynolds-averaging, *J. Hydr. Eng.*, **133** (9), 1074–1079.

Boussinesq J. (1877) Essai Sur la Théorie des Eaux Courantes (Essay on the Theory of Water Flow), *Mémories Présentés par Divers Savants à l'Académie des Sciences*, Paris, **23** (1), 1–680 [in French].

Carmo J. A. D. (2013) Boussinesq and Serre type models with improved linear dispersion characteristics: applications, *J. Hydr. Res.*, **51** (6), 719–727.

Castro-Orgaz O. and Hager W. H. (2014) One-dimensional modelling of curvilinear free-surface flow: generalised Matthew theory, *J. Hydr. Res.*, **52** (1), 14–23.

Chen C. L. (1991) Unified theory on power-laws for flow resistance, *J. Hydr. Eng.*, **117** (3), 371–389.

Cottino C. F. G. (1993) *An Experimental Study of Flow Around Bed Forms*, MSc Thesis, University of the Witwatersrand, Johannesburg, South Africa.

Delft Hydraulics Laboratory (1980) *Computation of Siltation in Dredged Trenches; Semi-empirical Model for the Flow in Dredged Trenches*, Report No. R1267-III/M1536, Delft, The Netherlands.

Dewals B. J., Erpicum S., Archambeau P., Detrembleur S. and Pirotton M. (2006) Depth-integrated flow modelling taking into account bottom curvature, *J. Hydr. Res.*, **44** (6), 787–795.

Dressler R. F. (1978) New nonlinear shallow flow equations with curvature, *J. Hydr. Res.*, **16** (3), 205–222.

Elder J. W. (1959), The dispersion of marked fluid in turbulent shear flow, *J. Fluid Mech.*, **5** (4), 544–560.

Fenton J. D. and Zerihun Y. T. (2007) A Boussinesq approximation for open channel flow, *Proceedings of the 32nd Congress*, *IAHR*, Venice, Italy, 2–6 July, CD-ROM, 1–10.

Fenton J. D. and Darvishi E. (2016) A discussion to "Minimum specific energy and transcritical flow in unsteady open-channel flow", *J. Irrig. Drain Eng.*, **142** (10), 10.1061/(ASCE)IR.1943-4774.0001077.

Ferziger J. H. and Peric M. (2002) *Computational Methods for Fluid Dynamics*, 3rd rev. ed., Springer-Verlag Berlin Heidelberg, New York, NY.

Fischer B. H., List E. J., Koh R. C., Imberger J. and Brooks N. H. (1979) *Mixing in Inland and Coastal Waters,* Academic Press, New York, NY.

French R. H. (2007) *Open Channel Hydraulics*, Water Resources Publications, Highlands Ranch, CO.

Ghamry H. K. and Steffler P. M. (2002) Effect of applying different distribution shapes for velocities and pressure on simulation of curved open channels, *J. Hydr. Eng.*, **128** (11), 969–982.

Haaland S. E. (1983) Simple and explicit formulas for the friction factor in turbulent pipe flow, *J. Fluids Eng.*, **105** (1), 89–90.

Hager W. H. and Hutter K. (1984) Approximate treatment of plane channel flow, *Acta Mech.*, **51**, 31–48.

James C. S and Cottino C. F. G. (1995) An experimental study of flow over artificial bed forms, *Water SA*, **21** (4), 299–306.

Jin Y. and Li B. (1996) The use of a one-dimensional depth-averaged moment of momentum equation for the non-hydrostatic pressure condition, *Can. J. Civ. Eng.*, **23**, 150–156.

Lyn D. A. (1993) Turbulence measurement in open channel flows over artificial bed forms, *J. Hydr. Eng.*, **119** (3), 306–326.

Massé P. (1938) Ressaut et ligne d'eau dans les cours d'eau à pente variable (Hydraulic jump and free-surface profile in channels of variable slope), *Rev. Gén. Hydr.* **4** (19), 1–11; **4** (20), 61–64 [in French].

Matthew G. D. (1991) Higher order, one-dimensional equations of potential flow in open channels, *Proc. Instn. Civ. Eng.*, London, England, **91** (3), 187–201.

Meyer-Peter E. and Müller R. (1948) Formulas for bed-load transport, *Proceedings of the 3rd Meeting of IAHR*, Stockholm, Sweden, 39–64.

Mohapatra P. K. and Chaudhry M. H. (2004) Numerical solution of Boussinesq equations to simulate dam-break flows, *J. Hydr. Eng*., **130** (2), 156–159.

Rodi W. (1993) *Turbulence Models and Their Application in Hydraulics: a state-of-the-art review*, IAHR monograph, 3rd ed., Balkema, Rotterdam, The Netherlands.

Serre F. (1953) Contribution à l'étude des écoulements permanents et variables dans les canaux (Contribution to the study of permanent and nonpermanent flows in channels), *La Houille Blanche*, **8** (6–7), 374–388; **8** (12), 830–872 [in French].

Shimozono T. and Sato S. (2016) Coastal vulnerability analysis during tsunami-induced levee overflow and breaching by a high-resolution flood model, *Coast. Eng.*, **107**, 116–126.

Sivakumaran N. S. (1981) *Shallow Flow over Curved Beds*, DEng Thesis, Asian Institute of Technology, Bangkok, Thailand.

Steffler P. M. and Jin Y. (1993) Depth averaged and moment equations for moderately shallow free-surface flow, *J. Hydr. Res*., **31** (1), 5–17.

Tossou E. E. (2009) *Extension of the 2DH Saint-Venant Hydrodynamic Model for Flows with Vertical Acceleration*, PhD Thesis, Laval University, Québec, Canada.

van Rijn L. C. (2011) *Principle of Fluid Flow and Surface Waves in Rivers, Estuaries, Seas and Oceans*, Aqua Publications, Amsterdam, The Netherlands.

White F. M. (2011) *Fluid Mechanics*, 7th ed., McGraw-Hill, New York, NY.

Zerihun Y. T. (2004) *A One-dimensional Boussinesq-type Momentum Model for Steady Rapidly-varied Open Channel Flows*, PhD Thesis, Department of Civil and Environmental Engineering, The University of Melbourne, Australia.

Zerihun Y. T. (2008) Development and validation of a one-dimensional non-hydrostatic open channel flow model, *Proceedings of the 31st Hydrology and Water Resources Symposium, and the 4th International Conference on Water Resources and Environment Research,* Adelaide, Australia, 15–17 April, CD-ROM, 2485–2495.

Zobeyer H. and Steffler P. M. (2012) Modelling plane open-channel flows by coupled depth-averaged and RANS equations, *J. Hydr. Res*., **50** (1), 82–88.